Plasmonic Nanobubbles as Transient Vapor Nanobubbles Generated Around Plasmonic Nanoparticles

Ekaterina Lukianova-Hleb[1], **Ying Hu**[2], **Loredana Latterini**[3], **Luigi Tarpani**[3], **Seunghyun Lee**[2], **Rebekah A. Drezek**[2], **Jason H. Hafner**[2], and **Dmitri O. Lapotko**[1,2,*]

[1]A. V. Lykov Heat & Mass Transfer Institute, 15 P. Brovka St., Minsk, 220072, Belarus

[2]Rice University, 6100 Main Street, TX 77005, USA

[3]University of Perugia, Via Elce di Sotto, 8, 06123 Perugia, Italy

Abstract

We have used short laser pulses to generate transient vapor nanobubbles around plasmonic nanoparticles. The photothermal, mechanical and optical properties of such bubbles were found to be different from those of plasmonic nanoparticle and vapor bubbles as well. This phenomena was considered as a new complex nanosystem – plasmonic nanobubble (*PNB*). Mechanical and optical scattering properties of *PNB* depended upon the nanoparticle surface and heat capacity, clusterization state, and the optical pulse length. The generation of the *PNB* required much higher laser pulse fluence thresholds than the explosive boiling level, and was characterized by the relatively high lower threshold of the minimal size (lifetime) of *PNB*. Optical scattering by *PNB* and its diameter (measured as the lifetime) has been varied with the fluence of laser pulse and this has demonstrated the tunable nature of *PNB*.

Keywords

vapor nanobubble; photothermal; scattering; pulsed laser; gold nanoparticle; plasmon resonance; vapor bubble

Plasmonic nanoparticles (*NP*) are known for their outstanding photothermal[1-6] and optical scattering[1,7-12] properties. These properties result from the interaction of *NPs* with optical radiation and the surrounding environment, and are characterized through their absorption and scattering cross-sections, respectively, which are well studied as a function of the parameters of *NP*, environment and optical radiation.[13-19] Since such interaction usually occurs in some medium (environment) the secondary thermal and hydrodynamic phenomena in such medium may significantly influence the properties of *NPs* as optical probes and heat sources. Short optical pulses and high-energy excitation of plasmonic *NPs* create transient and non-stationary thermal fields with vapor-liquid interfaces that significantly influence heat transfer from *NP* to its environment and create a strong gradient of the refractive index. In addition, vapor layers around *NP* cause blue shifts and attenuation of the extinction spectrum.[20] The multi-factor and non-stationary nature of the radiation-*NP*-vapor-liquid system complicates its experimental study and theoretical modeling. Available thermal models[6,17,21-24] are applicable mainly for continuous excitation and stationary heat transfer at low temperatures or for very short laser pulses (femto-second range), for a limited number of shapes of *NP*, and for temperatures that assume constant plasmonic cross-sections and are

*Rice University, Physics and Astronomy - MS 61, 6100 Main Street, Houston, TX 77005, Tel: 713-348-3708, Fax: 713-348-4150, dmitri.lapotko@rice.edu .

below the boiling threshold for the environment. Measuring a high transient temperature around individual *NPs* in a two-phase medium can be quite difficult if not impossible. Experimental methods[8,21-25] for monitoring the transient temperature of *NP* are applicable for sub-evaporation temperatures and for a single-phase medium or are applicable only to the suspension of *NPs*. These methods cannot characterize the local and transient effects of individual nanoparticles. Under high temperatures and possible melting of *NPs* and vaporization of its environment the photothermal and optical properties cannot be predicted using "cold" optical cross-sections of *NP* and thermo-physical properties of the surrounding liquid.

We hypothesize that high-temperature plasmonic interactions that involve localized transient evaporation of the environment around *NP* may create a new "*NP*-vapor-liquid" system, whose thermal, mechanical and optical properties would principally differ only from those of the plasmonic *NP*. Previous studies of the laser-induced bubbles focus on the phenomena that do not involve plasmon resonance as the bubble-generating mechanism: optical breakdown,[26-29] photothermal effect and ultrasound.[30-37] Although laser-induced macro- and micro-bubbles are extensively studied[27,28,36,38,39] and optical properties of acoustically and optically generated bubbles are well recognized,[30,31] the mechanisms of bubble generation (optical molecular absorbance on microscale, rarefaction and optical breakdown) do not provide the precise control of the bubble parameters at nanoscale. The lack of control over the bubble parameters may limit their important applications where the bubble mechanical, thermal and optical impacts require precise tuning and control at nanoscale. Although the femtosecond laser microsurgery methods have a high precision of mechanical impact[26,27,40] such methods also require very precise positioning of the laser beam waist relative to the target and this limits the application of the femtosecond methods.

Experimental studies of the bubble generation around plasmonic *NPs* include several reports, some of them being done with interesting methods.[2,13,14,16,23,41-44] However, these studies have two limitations: the bubbles were not detected directly or the individual *NPs* were not studied and these limit the accuracy of the data and the conclusions. Up to now, the thermal, mechanical and optical properties of plasmonic *NP*-generated environmental vapor nanobubbles have not been systemically analyzed.[4,5,14] In this work we study the properties of *NP*-generated transient environmental nanobubbles (that are in fact the event, not a particle) as functions of the properties of gold *NPs* (whose photothermal and optical scattering properties are relatively well characterized) and excitation laser radiation. To distinguish the origin and the scale of plasmonic *NP*-generated bubbles from nanoparticles and from vapor bubbles of other origin we define them as plasmonic nanobubbles (*PNB*).

RESULTS AND DISCUSSION

1. Generation of plasmonic nanobubbles have been studied around individual gold *NPs* in water by detecting the time-resolved scattering images and time responses from individual *NPs* exposed to the single optical pulses. The bubbles were quantified by measuring their lifetime (T_{PNB}), bubble generation threshold fluence (E_{PNB}) and the pixel amplitude of their scattering images. The lifetime of NP-generated bubbles has previously been found by us to be nearly proportional to the incident fluence for various types and sizes of investigated *NPs*.[45-48] Also, it was established by several groups theoretically[28,49-52] and experimentally[27,39,49] that the vapor bubble lifetime is proportional to its maximal diameter, which depends upon the energy deposited by *NP* into the bubble nucleus and characterizes its expansion/collapse dynamics. This allowed to used T_{PNB} as a measure of the mechanical (hydrodynamic) property of the *PNB*. Bubble generation threshold fluence (E_{PNB}) of the pump laser pulse describes both the efficacy of the photothermal conversion by *NP* and

hydrodynamic conditions of the bubble generation. It was defined as the minimal amount of the optical fluence required to support the bubble expansion around specific *NP*.

We have studied the influence of the *NP* size, heat capacity and surface; of the characteristic times of energy deposition (optical pulse length) and dissipation (thermal relaxation time). The properties of gold *NPs* employed (shells and spheres) where obtained from their manufactures. The diameters of *NPs* were verified using scanning and transmission electron microscopes. *NP* optical absorption and scattering cross-sections were calculated for specific shapes, dimensions and wavelength using previously verified Mie-based MATLAB code[10] (see Methods and Materials section). Individual gold *NPs* (spheres and shells) in water were irradiated with single pump laser pulses that caused water evaporation around laser-heated *NP* surface and the *PNB* generation (Figure 1). Heat capacity of the *NP* was varied by replacing the gold sphere by the gold shell with the same outer diameter though having the thin layer of gold outer core instead of solid gold interior. Duration of optical exposure varied from 0.5 ns (dual laser system STA-2H, Standa Ltd., Vilnius, Lithuania) to 10 ns (ND-Yag laser LS2132, Lotis TII, Minsk, Belarus), and to continuous irradiation (Uniphase 4301, San Jose, CA), all at the same wavelength of 532 nm. This pump wavelength has provided significant optical absorption by all studies of *NPs* regardless of their aggregation state or the position of the plasmon resonance peak. Despite the near-infrared peak for plasmon resonance of gold shells, their absorption cross-sections at 532 nm were found to be approximately 0.5 - 0.6 of its maximal value at the resonance wavelength (as measured with extinction spectra and independently calculated, see also the Methods and Materials sections). Gaussian pump laser beams were collinearly focused into 14 μm spot and individual particles (located in micro-cuvettes) were positioned in the beam center (Figure 1). The fluence of each pulse was calculated by measuring its diameter at the 0.5 level of the fluence maximum (by imaging laser pulse at the sample plane) and energy (by using calibrated photodetector). The diameter of gold *NPs* has been varied from 10 nm to 250 nm. Pulsed probe laser (690 nm, 0.5 ns, Standa laser system) was applied at the delay of 10 ns (relative to the pump pulse) for optical side-scattering imaging of *NPs* and *PNBs* with high sensitive digital camera (Luka, Andor Technology, Northern Ireland). Continuous low power probe beam at 633 nm (model 1145P, JDSU, Milpitas, CA and Melles Griot 905A stabilized laser) was directed collinearly with the probe laser and its side scattering was collected with 60x microscope objective with numerical aperture 0.8 and was monitored with FPD510A photodetector (Thorlabs, NJ) as a time response that has been used to measure T_{PNB} (at the 0.5 level of the maximal amplitude of the response).

Optical scattering images of the *NPs* (Figure 2A), the bubbles (Figure 2B) and time responses of the bubbles (Figure 2C) were acquired for individual *NPs* using single pump pulses. Comparing to the scattering image of intact *NPs* (Figure 2A) the Figure 2B has shown a significantly brighter image of one *NP* that was exposed to the pump laser pulse (the two other *NPs* shown at Figure 2A were not exposed to the pulse). Simultaneously we have detected the bubble-specific time response (Figure 2C).

Firstly we have estimated the threshold fluence for onset of explosive boiling[53] of water on the *NP* surface. We have used the hydrodynamic model[22] and the Stiffened gas equation of state[54] parameterized for water (see Sec. 2 in "Methods and materials" for details). The threshold fluence for the onset of explosive boiling was estimated as a minimal fluence for which the *NP* temperature reaches for the thermodynamic critical temperature for water(that is equal to 647 K.[55]) This model has not been designed to describe nanobubbles since the Stiffened gas equation of state does not take into account any phase changes and the thermal resistance of the *NP*-water boundary, which may create an additional temperature gradient at the boundary.[56,57] However, the nanosecond times considered in our study and a relatively big size of *NPs* (comparing to those analyzed in the cited above models) may smooth the

temperature jumps at the *NP*-water boundary and, therefore, the *NP* surface temperature should be close to that of water at the boundary. Obtained the estimates of the minimal laser fluence that results in a vapor near *NP* surface are presented at Figure 3. It should be noted that the actual onset of the explosive boiling may occur even at lower temperatures. [43,53,58,59]. and, therefore, our estimates show the maximal fluence. For 250 nm silica core-gold shells and solid spheres they turned out to be close (Figure 3). We have also considered the case of *NP* cluster, the group of closely located *NPs*, since the *NP* aggregation into a cluster is a common case for many applications. Plasmon properties of the *NP* cluster are different from those of an individual *NP*. However, it is difficult to precisely calculate absorbance cross-section of the cluster and thus to estimate its temperature. For this reason, we assumed that the initial heating of the *NPs* in the cluster was similar to the case of non-clustered *NPs* because the optical absorbance cross-section of individual shell in the cluster and at 532 nm should not significantly differ from that for a single shell. This assumption can be additionally supported by very broad absorption spectra of the employed *NPs* (250 nm gold nanoshells) and by using off-resonant wavelength of 532 nm for their excitation. Such conditions should be less influenced by their clusterization compared to the case of using the laser wavelength close to plasmon resonance and the *NPs* with sharp absorption peak. Spectroscopic studies of the water suspensions of the shells employed have shown further broadening of extinction spectra during their clusterization although without an apparent change of optical density at 532 nm (not shown). Our previous studies have shown the similar rule for the clusters of gold spheres[60]: *NP* clusterization has broadened the extinction spectrum rather shifted the narrow peak into the longer wavelength. Based on the above, we have estimated the boiling threshold fluence for the cluster as being the same as for a single shell *NP* (Figure 3). It was also very unlikely that the *NP* clusterization might increase the temperature of *NP* surface upon absorption of laser pulse.

Experimental measurements of E_{PNB} were based upon the detection of the smallest vapor bubble around individual *NP* (Figure 2B,C). Such measurements (performed simultaneously in image and in response modes) returned much higher thresholds than the above estimates (Figure 3). The measured E_{PNB} and calculated explosive boiling thresholds have yielded significant gaps for all studied *NP* shapes and dimensions. For example, for 250 nm gold spheres the difference between the E_{PNB} and the evaporation threshold was about 1 order of magnitude (Figure 3). For another type of *NP* – gold nanoshells – the observed E_{PNB} has been found to be almost 4 times higher than the threshold for explosive boiling. Clusterization of the *NPs* (clusters of 250 nm gold shells have been studied) has shown further decrease of the E_{PNB} relative to that for single shells (Figure 3). This can be explained by the formation of one joint vapor nucleus around all *NPs* due to merging of their individual vapor layers when all *NPs* are tightly coupled. In this case the bubble could start to expand from the nucleus having the size of the cluster.

To clarify the nature of the discovered differences in the boiling threshold and E_{PNB} we have designed additional experiments at the fluence level being close to the E_{PNB}. The amplitude sensitivity of the set up in the response mode was increased by more than one order of magnitude (by tight focusing the continuous probe beam onto the *NP* and directing this beam collinearly with the pump beam). In this mode we were able to detect the smallest bubbles due to the scattering of the probe beam by the bubble in all direction. Such scattering decreased the intensity of the probe beam at the photodetector resulting in a negative signal of *PNB*. Furthermore, the sensitivity of this mode was sufficient for detecting the heating of the water around *NP* (this caused an increase of the probe beam intensity at the photodetector due to "thermal lens" effect). Temporal resolution was improved to 1.2 ns by using 600 MHz/5 Gsample/s oscilloscope (X64, Lecroy Corporation) and the phototmultiplier tube module (Hamamatsu H6780-20).

This modification has allowed us to precisely monitor time responses around individual *NPs* in the transition range of pump laser pulse fluences (Figure 4). We have studied individual 80 nm gold spheres in water. At the sub-threshold fluence we have detected the response (Figure 4A) that is typical for heating (front length was about 1.5 ns that corresponds to the characteristic thermal relaxation time of the NP) and much longer tail that gradually approached the baseline (about 2 µs, not shown in full) that is typical for the cooling of the surrounding water due to thermal diffusion. We would like to note that this signal has been obtained for a single *NP*, not for ensemble. With the increase of the pump fluence (in very small increments) we observed the mixed responses that indicated two phenomena: heating and bubble generation (Figure 4B). The shortest detected bubbles have had a lifetime of 9±1 ns. Further increase of the pump fluence resulted in increase of T_{PNB} and in a total disappearance of the heating-related response (Figure 4C) starting from the T_{PNB} of 12-13 ns. The disappearance of the "thermal" response indicated that the temperature of the medium outside the *PNB* and after its collapse did not alter from an ambient level. Therefore, the smallest *PNBs* did not provide thermal insulation of the medium. This may be explained by assuming that the signals as shown in Figure 4B were caused by thing vapor layers near *NP* surface, and such layers did not prevent the heat transfer to surrounding water. Simultaneous monitoring of optical scattering from the same *NP* with the pulsed probe laser has shown the attenuation of the scattering by such small bubbles relative to the scattering of the intact *NP* (Figure 5).

However, the increase of the T_{PNB} to 12-13 ns (and corresponding increase of the maximal diameter of the bubble) has resulted in the amplification of optical scattering (Figure 5). Optical scattering properties of *PNB* are considered in detailed in the next section and here we focus on the mechanism of *PNB* generation. We have plotted the T_{PNB} (measured as the duration of the *PNB*-shaped response) and the bubble generation probability (measured as the ratio of the *PNB*-shaped responses to the total number of the studied *NPs*) as the function of the pump laser fluence (Figure 5). Both parameters have yielded a discontinuity at a specific fluence: no bubble-specific signals were detected at lower fluence, while at the fluence above the threshold level the both parameters increased with the fluence (readers interested in T_{PNB} versus fluence functions for a wider ranges of the pump pulse fluences and *NP* types and dimensions may find such data in our previous publications[46,60]). This increase has started not from zero but from the minimal threshold level (Figure 5). We have studies 250 nm gold spheres and have found the similar results: minimal T_{PNB} was 9±1 ns and the function T_{PNB} vs fluence had the similar step discontinuity at the E_{PNB}. This result has been observed for all studied *NPs* (spheres 10 - 250 nm, shells 60 and 250 nm) and for their clusters.

The discovered discontinuity of the T_{PNB} (and hence of its maximal diameter) does not match classical understanding of the vaporization and bubble formation near heated surface that predicts gradual decrease of the bubble lifetime to zero with much lower fluence threshold (as shown with the dashed red line in Figure 5). Such gradual decrease to zero lifetime was reported before,[61] even for the suspensions of gold NPs[47] and is considered to be a general rule when the bubbles are generated in heated medium. In contrast, our results showed the existence of rather high fluence threshold; furthermore, small bubbles seemed not to be "allowed" to be generated around *NPs* even at the fluences that are sufficient for vapor formation near *NP* surface.

To further validate this assumption we have performed an additional experiment by replacing *NPs* with homogeneous optically absorbing molecular solution of Trypan Blue. All experimental conditions were identical. We have detected a heating-cooling type of the response (Figure 4D). The sign of this response was opposite to the *NP* case because much larger area was heated (its diameter was several micrometers and was determined by the

cross-section of the pump laser beam). Then we gradually increased the fluence until we have detected the bubble-shaped component in the response (Figure 4E). The generation of the bubbles in this case has had a photothermal mechanism due to the laser-induced heating of all medium. The minimal duration of the component associated with the photothermal bubble was found to be 1.6 ns (comparable to the temporal resolution of the experimental set up) and has gradually increased with fluence (Figure 4F) without any discontinuities as were discovered for PNBs. Therefore, we concluded that the mechanism of the generation of *PNBs* is different from current understanding of the bubble generation and the evaporation of water near *NP* may not be sufficient for the bubble expansion. Furthermore, small bubbles cannot be generated around plasmonic *NPs* at the fluences that correspond to the temperatures above explosive boiling threshold. Additional deposition of thermal energy was apparently required to support the expansion of the bubble. This feature of *PNBs* has apparently increased the fluence and temperature thresholds for the *PNB* generation relative to those associated with explosive boiling thresholds. For micro- and macro-absorbers the formation of vapor coincides with the beginning of vapor bubble expansion (like shown at Figure 4E). However, it appears that this rule does not work for *PNBs*.

Since we consider the bubble as a hydrodynamic phenomenon, the beginning of its expansion from the vapor layer requires overcoming an outer pressure. At nanoscale and around *NP* surface such pressure may significantly increase due to the effect of the surface tension. Surface tension pressure is known to be inversely proportional to the radius of curvature of the liquid-gas interface,[62-64] and the decrease of a diameter of the bubble nucleus (which can be roughly approximated by the size of *NP*) from 10 μm (relatively well characterized case for the micro-bubbles) to 100 nm (case of nanobubbles) will cause a 100-fold increase in the surface tension pressure. This additional pressure can be estimated with Young-Laplace equation[62] and for 250 nm *NP* is about 11 atm. We have studied this effect by varying the diameter of the *NP*. Obtained results are shown at Figure 6 for gold spheres and shells.

We have found that an increase of the *NP* diameter from 10 nm to 80 nm (solid gold spheres) has lowered the E_{PNB} by 18 times. This may be attributed to the decrease of the surface tension pressure as the latter is inversely proportional to the *NP* diameter. For example, comparing to the flat surface, an additional pressure due to surface tension around the 10 nm *NP* can be estimated by 280 atm., and for the 80 nm *NP* by 35 atm. (8 times lower than the 10 nm *NP*). At the same time the estimates of the evaporation thresholds (that also took into account the change of optical absorbance cross-section of *NPs* with diameter at the pump laser wavelength) have not shown the similar trend for the explosive boiling threshold fluence (Figure 6) because this threshold cannot be influenced by the surface tension and depends upon optical absorption cross-section and thermo-physical properties of *NP* and *NP*-water boundary. The 6-fold decrease of the explosive boiling threshold (for 60 nm *NPs* versus 10 nm *NPs*) can be explained by the increase of the ratio of absorption cross-section to geometrical cross-section of *NP* with the size (see Methods and Materials section). Therefore, the influence of *NP* size on the explosive boiling threshold and on the E_{PNB} was significantly different. The increase of *NP* diameter from 10 nm to 80 nm has decrease the explosive boiling by 6 times against 18 times for the bubble generation.

Based on the known dependence of the surface tension pressure of liquid-vapor interface upon the radius of such surface[62] we may assume that overcoming surface tension pressure requires increasing the pump laser fluence by almost two orders of magnitude above the boiling threshold for small *NPs*. As the *NP* size increases the limiting effect of the surface tension decreases. This can be seen from the analysis of the ratio of explosive boiling threshold to the E_{PNB} as a function of the *NP* size (dashed line at Figure 6). This ratio has gradually increased with the size of *NP* from 0.01 (for 10 nm sphere) to 0.1(for 250 nm

sphere). We may expect that these two thresholds converge for micro-absorbers and micro-bubbles as it was previously observed for evaporation and bubble expansion at micro-scale. Possible double-threshold mechanism of the generation of *PNB* and the limitation on the minimal T_{PNB} (and hence of its maximal diameter) may be important in any application of photothermal plasmonic effects associated with the two-phase transient conditions at nanoscale.

The increase of the *NP* diameter above 80 nm has caused some increase in the E_{PNB} for the spheres (Figure 6): the E_{PNB} for the 250 nm sphere was 1.3 times higher than that for the 80 nm sphere. This reverse trend may be explained by the effect of an increased heat capacity for gold spheres. However, the increase of the E_{PNB} was not observed for the shells (Figure 6), whose heat capacity was lower than that for the spheres of the same diameter. The combination of big diameter and low heat capacity of 250 nm silica-gold shell has provided the lowest level of the E_{PNB} of 42 mJ/cm^2 for individual *NPs* (Figure 6).

Another important property of *NPs* that influences the E_{PNB} is the *NP* heat capacity and the surface of heat transfer between the *NP* and water. For three objects presented at Figure 3 the ratio of the surface of heat exchange to the heat capacity gradually increased from sphere to shell and from shell to shell cluster. The influence of these factors was analyzed in terms of T_{PNB} measured under identical excitation conditions (0.13 J/cm^2). Decrease of the heat capacity of an individual *NP* (shell versus sphere) and increase of the heated surface (shell cluster versus individual shell) have significantly increased the T_{PNB} that characterizes the maximal diameter of *PNB* (Figure 7). We have found that under equal conditions the shells of 60 nm and 250 nm diameters have generated the *PNBs* more efficiently compared to solid spheres of the same diameters. It should be noted that the pump wavelength of 532 nm has much better matched plasmon resonance for the spheres rather than for the shells (the latter have near-infrared plasmon resonance peak). Even despite this disadvantage the shells have provided the most efficient generation of *PNB* as well as the lowest thresholds fluences of *PNB* generation.

NP clusterization has lowered the E_{PNB} (Figure 3) and has improved the T_{PNB} (Figure 7). We assumed that the clusterization might have caused the formation of one joint vapor nucleus around all *NPs* due to merging of their individual vapor layers when all *NPs* are tightly aggregated. In this case the bubble could start to expand from the nucleus with the size of the cluster. The bubble generation from the nucleus with increased size should have required less energy compared to that for single *NP* since an increased diameter results in lower surface tension pressure. This explained the decrease of the E_{PNB} as shown in Figure 3 and increase in T_{PNB} under identical excitation conditions as shown in Figure 7. At the same time the heat capacity of the *NP* cluster should be smaller than that for the one solid sphere of the same diameter as the cluster. Our previous studies have shown that the clusters of 30 nm gold spheres were much more efficient for generating the nanobubbles than the single spheres of the diameter being close to that of the cluster (250 nm solid spheres).[46] It is interesting to note that the time response of the cluster-generated bubble has had the same shape as the response of the bubbles generated around individual *NP* (Figure 2C). Therefore, the cluster has acted as a solid thermal source and has generated one bubble, not many individual small bubbles around single *NPs*.

The next studied factor was the duration of optical excitation that is related to the losses due to thermal diffusion. We have studied this factor theoretically and experimentally for 250 nm shells (as the most photothermal efficient *NPs*). Individual shells were exposed to the single pulses of 0.5 ns and 10 ns and also to a continuous laser at the same wavelength (532 nm). E_{PNB} has significantly increased (by one order of magnitude) with the increase of the duration of the laser pulse (Table 1). Furthermore, continuous excitation during 10-100

seconds at the intensity up to 30 kW/cm^2 (maximal available from the laser) has yielded no bubbles at all around single *NPs*. Estimated explosive boiling threshold was found to be about 380 kW/cm^2 (calculation of the threshold fluence for continuous excitation is described in the Method and Materials). Such intensity exceeds damage thresholds for many substances, especially biological ones. This brings us to the conclusion that the generation of the bubbles around the individual *NPs* is not optimal with continuous lasers and requires rather short pulsed excitation.

Observed effects of the laser pulse duration can be attributed to the two processes: a thermal dissipation and formation of vapor bubble. Only the length of the 0.5 ns pulse was comparable to the characteristic time of the thermal relaxation for 250 nm shells (0.4 ns approximately), and this pulse has provided the best conditions for accumulating thermal energy around *NP*. Longer optical exposure time was accompanied by significant thermal dissipation from the *NP* and had to be compensated by the increase of the laser pulse fluence so as to maintain the bubble generation temperature at the *NP* surface. This might have caused an increase of the both thresholds: of explosive boiling and of the E_{PNB} (Table 1). However, these two thresholds have responded differently: the ratio for bubble generation/ explosive boiling thresholds has decreased from 0.31 (0.5 ns pulse) to 0.1 (10 ns pulse) as shown in the Table 1. This can be explained by an additional screening (scattering) of *NP* by the surrounding bubble, which resulted in an additional decrease of the incident pump fluence at the *NP* surface, which, in turn increased the fluence level required to support the bubble generation. The emerging nanobubble created additional losses of optical energy (of the pump pulse) since it might scatter the incident pump beam[44] and, additionally, might decrease an absorption cross-section of the *NP* by lowering the refractive index of the surrounding medium[20]. Since the time of the formation of the bubble nucleus is relatively short (about 0.05 - 0.1 ns [42,43,53,58]) the above effects also indicated that the photothermal efficacy of *NP* was no longer constant and depended upon the dynamics of the surrounding bubble.

Explosive boiling threshold was found to be less sensitive to the duration of optical exposure (Table 1). It has increased by 3 times, not by 10 times as the E_{PNB}. This additionally shows that the formation of vapor near *NP* surface and the bubble generation are the different phenomena at nanoscale. Another *PNB* parameter – its T_{PNB} – was obtained at the identical fluence of the short and long pulses (Table 1). The 10-fold shortening of T_{PNB} under excitation with a long pump pulse has correlated with the increase of the E_{PNB}. These results showed lower efficacy of longer pulse the generation of *PNB*. Furthermore, a vapor nanobubble may significantly influence photothermal properties of plasmonic *NP* (located inside the *PNB*) and this effect requires further detailed studies (that are beyond the scope of current work).

2. Optical properties of plasmonic nanobubbles are related to their diameter and were analyzed with the time-resolved side scattering imaging by using time-delayed probe laser pulse (0.5 ns, 690 nm). Due to the small diameters of *NPs* and bubbles their scattering images represented diffraction-limited spots (Figure 2A,B). Pixel image amplitude in the center of such spot was measured as I_{sc}. To quantify optical efficacy of the nanoparticle-generated bubble relatively to that of the *NP* alone we have analyzed optical amplification coefficient K_{amp}:

$$K_{amp} = (I_{sc}(t) - I_{bc}) / (I_{sc}(0) - I_{bc1}),$$

where *t* is the delay time of the probe pulse relative to the pump pulse (10 ns) and zero time corresponds to the scattering by of an intact *NP* alone prior to its exposure to a pump pulse,

I_{bc} and I_{bc1} are the background pixel amplitudes. Subtraction of the background has provided correct quantities comparison of the experimentally measured levels of optical scattering. All data were obtained under the fixed gain of the camera. K_{amp} indicates amplification or attenuation effect of the bubble on optical scattering relative to that of gold *NP* and characterizes the relative sensitivity of the *PNB* as optical probe compared to that of *NP*. In many applications it is also important to estimate the specificity of imaging. We defined the contrast coefficient K_{spec} as the ratio of scattering image pixel amplitudes obtained for the two different objects under identical illumination conditions:

$$K_{spec} = (I_1 - I_{bc1})/(I_2 - I_{bc1}),$$

where the indexes 1 and 2 indicate the two different objects that were identically irradiated by the pump and probe laser beams. The *PNBs* were generated with a single pump pulse. Their image and time response were obtained simultaneously. Figure 8A shows experimentally obtained optical amplification coefficients as a function of the pump fluence for the *NPs* of various diameter and structure. Dashed vertical lines show the for each *NP*. Both shells and spheres have demonstrated quite similar attenuation of the scattering amplitude for sub-threshold pump fluences. No bubbles were detected under such conditions and *NP* scattering images were apparently dimmed during NP exposure to the pump laser pulse. Based on the estimated explosive boiling threshold fluences we suggest that the vapor layers were formed around heated *NPs* though these layers were unable to expand into bubbles due to the limiting action of surface tension. These layers might have caused an observed attenuation of optical scattering relative to that of *NPs* by shifting plasmon resonances of gold *NPs*[25] (when water was replaced by vapor) and through the destructive interference of the incident and scattered probe laser radiation. Our modeling of the scattering by *NP* in water and by the *NP* surrounded by the vapor has shown similar attenuation effect for the thin vapor layer around the *NP* (Figure 8B).

Further increase of the pump laser fluence has resulted in apparent amplification of scattering (Figure 8A). Amplification coefficients gradually increased with pump laser fluence for all studied *NPs*, which can be explained by the effect of the bubble diameter: the higher the fluence, the bigger the bubble, and thus the stronger the scattering. We have previously studied the amplification effect in detail recently for gold spheres.[67,68] However, for shells this effect was found to be even stronger (Figure 8A) and this perfectly correlates with the discussed above photothermal properties of the shells: under identical fluences the shell generated much bigger bubble comparing to that generated by the sphere, so the shell-bubble system has yielded higher optical amplification comparing to the sphere-bubble system.

Also, 60 nm particles have yielded much higher optical amplification comparing to the 250 nm particles for the same level of pump laser fluence (Figure 8A, Table 2). This can be explained by lower initial levels of scattering by the *NPs* alone (Table 2): for the 60 nm *NPs* they were 8-10 times lower than those for 250 nm particles and hence, K_{amp} for smaller *NPs* was higher. This experiment has shown that the sensitivity of optical scattering imaging can be improved by two orders of magnitude and our calculations show that this parameter can potentially increase up to three orders of magnitude relative to the scattering of gold nanoparticles.

Next, we have measured the *PNB* scattering image pixel amplitudes as a function of T_{PNB} (Figure 9A) that directly characterizes maximal diameter of the bubble. This process was modeled by calculating optical scattering cross-sections of the nanoparticle-bubble system as the function of the bubble radius (Figure 9B). We have noticed several interesting trends:

1. There was a relatively good correlation between T_{PNB} and the amplitude of its scattering image (the values of the Pearson correlation coefficients were found to be 0.94 for 250 nm shells, 0.93 for 250 nm spheres, 0.86 for the 60 nm shells and 0.85 for 60 nm spheres);

2. Experimental dependences of the bubble image amplitude versus T_{PNB} (Figure 9A) showed qualitative agreement with theoretically obtained dependences of the bubble scattering cross-section versus bubble diameter (Figure 9B);

3. Scattering image amplitudes of the nanoparticle-bubble system almost did not depend upon the NP size and type starting from the T_{PNB} of 25 ns (Figure 9B, Table 2).

Therefore, we conclude that the optical properties of the *PNB* were determined by properties of the bubble rather than by those of the plasmonic *NP*. This result is in line with previously reported optical scattering properties of the bubbles that were acoustically and optically generated in homogeneous media without *NPs*.[20,30] Obtained data have also demonstrated that optical efficacy of *PNB* can be tuned with bubble size, which can be done by varying the pump pulse fluence. Significant amplification has a transient nature and this nature of the *PNBs* makes them highly flexible optical probes that can be activated and tuned on demand in real time. For a better control of plasmonic nanobubble scattering, two optical sources should be employed: besides the source for illuminating the scattering object (probe laser beam) an additional optical source is required for the excitation of the bubbles (pump laser beam). Also, since the bubble scatters the pump optical radiation, the pump pulse can be used for imaging as a single optical source (though with lower sensitivity) for imaging.

The specificity of *PNBs* as optical probes was studied with four different *NPs* (Figure 10). All data were obtained at the same level of pump laser fluence – 0.13 J/cm^2. This fluence was above the E_{PNB} for the 250 nm and 60 nm shells and 60 nm spheres, and corresponded to the E_{PNB} for 250 nm spheres. All *NPs* with the above bubble generation threshold conditions have yielded significant amplification of optical scattering in the range from 17 to 113 (Table 2), while for the 250 nm spheres (bubble generation threshold conditions) we have observed attenuation of scattering. We have compared optical contrast coefficients K_{spec} for the pairs of the two different *NPs* with the contrast coefficients K_{spec} for the *PNBs* generated around these *NPs* (Figure 10). As defined above the contrast coefficient shows the ratio of image pixel amplitudes for two objects that are identically illuminated and thus characterizes the contrast of these two objects relative to each other. The generation of *PNBs* around *NPs* has caused up to 200-fold increase or decrease in optical contrast coefficient as compared to the scattering by *NPs* alone: the amplitude of scattering by 60 nm shell has been very low compared to that by big 250 nm sphere (*Kspec* is 0.048) while the exposure of these two nanoparticles to a pump laser pulse with the fluence 130 mJ/cm^2 has generated the *PNBs* that have, respectively, decreased scattering by 250 nm sphere and increased the scattering by 60 nm shell thus increasing the optical contrast coefficient from 0.048 to 9.5 (Figure 10). This was achieved with the attenuating and amplifying effects of the *PNB*, which optical scattering has dominated the scattering effect of gold nanoparticle.

3. Comparison of the properties of *PNB* and other vapor bubbles

Obtained results have yielded some common and some totally different features of *PNB* when compared to those of vapor bubbles generated at micro-and macro-scale through photothermal and other mechanisms.

The influence of the surface tension on the bubble generation threshold at nanoscale has been predicted also for "classical" bubbles in [69] as an increase of the bubble generation threshold temperature relative to the micro- and macro-scale. Furthermore, such dependence

of the threshold temperature upon particle size has been observed experimentally even for relatively big melanosomes.[70] In case of plasmonic *NP* the influence of surface tension may be accompanied by another effect: attenuation of the incident fluence of the pump pulse at the *NP* surface due to increasing optical scattering of the pump laser radiation by the bubble developing around *NP*. Similar effects have already been observed earlier for the ensembles of gold *NPs*[44] and for the gold clusters on glass substrates.[71] The latter result has also shown the increase of the E_{PNB} relatively to the explosive boiling threshold. Due to the bubble dynamics the optical scattering of the pump radiation depends upon duration of laser pulse and is discussed in detail below. Nevertheless the combined action of these two factors (surface tension pressure and optical scattering of the pump laser pulse) seems to be unique for plasmonic *NPs*.

The major discovered difference is associated with the discontinuity of T_{PNB} and size (Figure 5). Small and short-lived *PNB* seemed not being allowed unlike the photothermal bubbles that can be much smaller and shorter under similar conditions (Figure 4E).

Next, *PNB* has never shown any thermal phenomena after its collapse that occur after the collapse of the "classical" bubbles due to extreme and fast decrease of the bubble volume at the final stage of its collapse: heat release, shock waves and sonoluminescence. In contrast the *PNBs* have demonstrated the absence of these phenomena in the whole range of studies conditions. *PNB* is limited spatially by the surface of *NP* (which is much bigger than the terminal volume of the free bubble at the last stage of its collapse) and thus the *NP* prevents the above extreme phenomena. The absence of heating of the medium outside the *PNB* implies that its major impact on the environment can be attributed to mechanical effect of the expanding bubble. Although the thermal insulation properties of vapor bubbles have been discussed previously[43,53,72] we have experimentally demonstrated this effect in quantitative and direct way and for the individual plasmonic *NPs*.

The mechanical impact is determined by the maximal diameter of *PNB* that is almost linearly proportional to it T_{PNB}. The latter property of the bubble has been initially established by Rayleigh theory[50] and later has been confirmed for nanobubbles.[27,73,74] Based on the cited above data we may estimate that the lifetime of 100 ns corresponds to the maximal diameter in the range from 500 nm to 1000 nm. According to our results, this property of *PNB* can be precisely tuned by varying the fluence of the pump laser pulse (Figure 5). Our results show that by tuning the T_{PNB} with the fluence of the pump laser pulse we can precisely control the mechanical impact of *PNB* at nanoscale and around specific *NPs*.

Finally, the *PNB* time response was found to be symmetrical for short lifetimes (Figure 2C and Figure 4B) and with the increase of the T_{PNB} the tail became longer than the front (Figure 4C). This asymmetrical effect can be attributed to the discussed above thermal insulating action of the bubble that in turn might force the *NP* to store thermal energy. Thus the *NP* could feed the bubble during its evolution and long after the termination of the laser pulse. The time shape of the photothermal bubbles was found to be either also symmetrical (Figure 4F) or, for the bigger bubbles, the tail became shorter than the front[75] due the energy losses.

All discussed differences imply that plasmonic *NP* plays an important role in the mechanism of bubble generation resulting in unique properties of the system that we referred as to plasmonic nanobubbles. A relatively high number of the bubble-related publications (including some cited above) considered the bubble generation with laser pulses of nanosecond and longer durations. Even higher number of the publications considered photothermal effects of plasmonic *NPs* (regardless the bubbles) under continuous excitation,

which resulted in a bulk thermal effect and required a significant amount of *NPs*. However, the most efficient nano-scale photothermal effect of individual *NPs* assumes sub-nanosecond pulses and is in good agreement with the one of the basic works on localizing photothermal effects of absorbed laser radiation.[65] Further shortening of optical pulse below an acoustic relaxation time would inevitably cause the generation of pressure and shock waves generated by $NP^{36,46,66}$ (while not excluding the generation of the bubbles) and may cause an optical breakdown.[26] The latter phenomenon can also generate vapor bubbles, but such bubble would be generated by plasma instead of *NPs* and the mechanism of the bubble generation is different since *NP* and plasma create different nuclei. When the bubbles are generated through optical breakdown or through the optical absorbance by the bulk medium the size of the bubble nucleus is determined by dimensions of the excitation laser beam (focal waist) and is expected to be significantly larger (1-2 orders of magnitude) than the diameter of *NP*. Obtained results show that the mechanism of *PNB* generation is different from that for macro and micro-bubbles in optically absorbing medium. Our studies of the *PNB* generation process can be resumed by the following: (1) the generation of vapor nanobubbles around heated plasmonic *NPs* is likely to involve the two-stage mechanism with the first stage being the vapor formation around *NP* surface and the second stage being the hydrodynamic expansion of the vapor nanobubble; (2) there is a certain limitation on the minimal T_{PNB} (around 9-10 ns); (3) for the excitation laser pulse being not longer than the thermal relaxation time of the bubble source E_{PNB} and maximal diameter of *PNB* (its T_{PNB}) are determined by the NP size, heat capacity and aggregation state. The main difference of *PNBs* from heated plasmonic *NPs* can be resumed by the threshold and tunable nature of thermal, mechanical and optical effects of *PNB* and by its transient nature (table 3).

CONCLUSIONS

The results reported above are quite preliminary and require further studies. However, we can conclude that the interacting plasmonic nanoparticle and vapor-water environment represent one complex nano-system that combines plasmonic properties of the NP with optical and hydrodynamic properties of vapor nanobubble. This system, defined by us as a plasmonic nanobubble, has the optical scattering properties different from those of plasmonic nanoparticle and hydrodynamic properties (including the mechanism of the bubble generation) different from those for the other types of optically and acoustically induced vapor bubbles. The reported results were obtained with the experimental methods developed by us that have enabled the study of heating and evaporation around individual transiently heated NPs. We conclude that:

1. The generation of plasmonic nanobubble does not coincide with the formation of a vapor around the surface of transiently heated plasmonic nanoparticle and requires additional energy that significantly exceeds the explosive boiling threshold. This additional and higher threshold also resulted in the limitation of the minimal lifetime (and hence maximal diameter) of the *PNBs* at the level of 9 ns. The possible explanation of the discovered mechanism of *PNB* generation may relate to the surface tension pressure applied to the vapor nucleus near the nanoparticle surface.

2. Plasmonic nanobubble generation threshold fluence is determined by nanoparticle size, heat capacity, aggregation state, and the pump laser pulse duration. Low *PNB* generation threshold fluence can be achieved with *NPs* with high ratio of the surface to heat capacity (such as in nanoshells), through *NP* clusterization and through the shortening of laser pulse to the level below characteristic time for thermal relaxation of the *NP* or their cluster.

3. Optical scattering and mechanical properties of the plasmonic nanobubble above the generation threshold can be tuned through the fluence of the pump laser pulse thus providing precise control of plasmonic nanobubbles.

METHODS AND MATERIALS

Experimental set up

Optical generation and detection of the nanobubbles was performed with previously developed by us photothermal laser microscope[46] equipped with the two pulsed lasers. In our work we have employed a pulse of length 10 ns, 532 nm (Nd-Yag LS2132, Lotis TII, Minsk) and a much shorter subnanosecond pulse of 0.5 ns at the same wavelength (STA-01 SH, Standa Ltd, Vilnius). Two pumping laser beams were directed into the illumination path of an inverted optical microscope and were identically focused into the sample chamber with a water suspension of gold NPs (Figure 11). The pulse fluence was varied by rotating the Glan prism and was measured using an Ophir energy meter (Ophir Optronics, Ltd., Israel) and an image detector (Luca, Andor Technology, Ireland). The latter provided imaging and direct measurement of the actual diameter of the laser beam. A *NP* sample was irradiated at several different locations (with a single *NP* or *NP* cluster in the center) one by one with a single focused laser pulse (diameter 14.0 μm) at fixed fluence level by scanning the sample mounted on the microscope stage. The concentration of the *NPs* was adjusted so as to avoid the overlapping of the laser induced thermal fields with the bubbles. Such a setup has ensured that a single *NP* and a single event were studied. Individual single nanoparticles were irradiated with single pump laser pulses.

Imaging of *NPs* and nanobubbles was realized by using side illumination of the *NP* sample with a pulsed probe laser beam at a wavelength (690 nm) different from the pumping laser wavelength (532 nm). A short probing pulse with a duration of 0.5 ns and with a tunable time delay relative to the pumping pulse provided time-resolved imaging of a short-living scattering object such as vapor bubble (Figure 11). Optical scattering is also used for the imaging of metal *NPs* and their clusters. We may expect that the scattering from bubble would amplify the amplitude of the scattered light relative to that from *NP*, because the diameter of a bubble is larger.

While allowing to "see" the vapor bubble the pulsed imaging cannot provide kinetic measurement. The latter was realized by the thermal lens method in a response mode. An additional continuous probing beam (633 nm) was directed to the sample and focused on it collinearly with pumping laser beams (Figure 11) and its axial intensity was monitored by a high-speed photodetector (PDA110AC, Thorlabs Inc.) and 200-MHz USB digitizer. The bubble-induced scattering of a part of the probing beam decreased its axial amplitude resulting in a dip-shaped output signal. This method also allows the detection the thermal field as they create local gradients of the refractive index in the beam path. The response mode allowed measurement of the bubble lifetime that characterizes a maximal diameter of the bubble. Image and response modes were used simultaneously thus combining the imaging and measuring of the lifetime. The bubble-related optical signal can be detected from a zero level when the light scattered by the bubble in the specific direction is registered and thus produces the positive signal that characterizes the angle-specific scattering effect. Alternatively, the probing beam can be directed into the sensor thus producing some base-level signal. The scattering by the bubble in all directions would decrease the amount of light at the detector thus producing the negative signal that characterizes the integral scattering effect. Also, besides the pulsed probing beam the continuous illumination and detection can be used so to register a kinetic behavior of the bubble. We defined the continuous optical monitoring of the bubble as a response mode and the time-resolved pulsed imaging of the bubble as an image mode.

Samples

Gold nanoparticles were obtained and fabricated as described below. Gold spheres of 10, 30, 80 and 250 nm diameter were obtained from Ted Pella Inc (Redding, CA). Gold spheres and hollow gold shells of 60 nm diameter were obtained from Nanopartz (Salt Lake City, UT). Gold shells of 250 nm diameter and with silica core inside were prepared as described previously.[76-78] The growth of the shell was checked by the means of optical spectroscopy. The morphology of the shells was analyzed by scanning electron and transmission electron microscope.

NP clusters were prepared by adding 40% volume of an acetone into the suspension of *NPs* and re-suspending the clusters in water so to adjust their concentration to that of the single *NPs*. Formation of the clusters has been verified with the three methods: with optical spectroscopy, by electron microscopy, and optical scattering microscopy. The number of *NPs* in the cluster was quite heterogeneous parameter and for this reason we have obtained data for the 40-60 objects that were averaged. We have used optical scattering amplitude (measured with the camera) as the relative measure of the cluster size: only the objects with the close optical scattering amplitudes were used for the experiments.

Water samples of gold *NPs* were prepared on standard microscope slides and coverslips of 18 mm diameter. Glass coverslips were cleaned using piranha solution, completely rinsed with deionized water, and dried with a stream of nitrogen gas. This procedure has provided very clean surfaces of the coverslips, which was critical for optical scattering imaging since the samples were used with the coverslips being under the slide glasses. The sample has been prepared by adding 1 μl polysterene microspheres of 10 μm diameter (Spherotech Inc., Lake Forest, IL) to 4 μl of the *NP* suspension. These microspheres have been used as spacers between the two glasses so to provide specific height (10 μm) of the sample volume. The concentration of gold *NPs* was adjusted to provide their low surface density (1 nanoparticle as per 100-200 μm^2) so to exclude the exposure of closely located nanoparticles to laser irradiation. The coverslips then have been sealed with Permount to prevent evaporation of the sample. The objects (*NPs* or *NP* clusters) were positioned into the center of laser beam with the help of side scattering imaging.

Modeling of laser-induced heating of the *NP* in water

In this quite approximate model, heating of a *NP* is assumed to be homogeneous. The *NP* temperature is determined by the differential equation accounting for the cooling of a *NP* by the surrounding water. The effects of thermal expansion of the *NP* are found to be small for nanosecond laser pulses and not taken into account. Thermal and dynamic processes in water are described by the Navier-Stokes equations accounting for the water compressibility. Thermodynamic properties of water were calculated with the help of the Stiffened gas equation of state[54] parameterized for water.[22] The Navier-Stokes equations are solved numerically with the help of a *TVD* (Total Variation Diminishing) scheme[79] generalized for the complex equation of state for real water. The threshold fluence for vapor formation near *NP* surface is determined with the help of this model as a fluence for which the maximal particle temperature that is achieved during laser heating is equal to 647 K – critical temperature for surrounding water. The equations of the model were solved numerically with the help of *TVD* schemes generalized for the complex equation of state for real water. The model employed did not consider real bubble dynamics since it does not account for mass and heat exchange processes and surface tension on moving spherical vapor-liquid interface, the dynamics and heat transfer in the supercritical fluid adjacent to the gold nanoparticle. Also this model does not account for the thermal resistance of the *NP*-water boundary, though for the times and *NP* sizes considered the temperature gradient at the boundary can be expected to be minimal. This model, being quite rough, however,

allowed us to estimate the laser pulse fluence threshold that is associated with the formation of vapor at the *NP* surface. Our model estimates of the threshold for the onset of the evaporation near *NP* surface did not count for the thermal resistance at the *NP*/water boarder that causes much lower temperature of the water relative to that of the *NP*. However, it has been shown that this difference is a short living phenomenon and it may vanish by the time comparable to the pump pulse length (500 ps).[43]

For continuous excitation of a *NP* in a medium, one can estimate the threshold intensity $I_{L(e)}$ for the onset of explosive boiling of the surrounding medium on the *NP* surface assuming that the flux of the absorbed laser energy is equal to the heat flux from the particle to the surrounding medium, i.e.

$$2\pi R_p \kappa_m Nu\left(T_p - T_\infty\right) = \sigma_{pa} I_{L(e)},$$

where T_∞ if the medium temperature far enough from the NP surface, $T_p = T_\infty + 274$ °C is the particle temperature, R_p and σ*pa* are the particle radius and absorbance cross-section, respectively, κ_m is the thermal conductivity of the surrounding medium, and $Nu = 2$ is the Nusselt number for the steady-state heat exchange problem on a spherical surface.

For a gold *NP* with $R_p = 125$ nm and $\sigma_{pa} = 6.81 \times 10^{-10}$ cm^{-2} in water with $\kappa_m = 0.6$ Wm^{-1}K^{-1},[79] this equation predicts that the threshold fluence is equal to $I_{L(e)} = 380$ kW cm^{-2}.

Calculation of optical cross-sections of *NPs* and modeling of optical scattering

NP optical absorption and scattering cross-sections were calculated for specific shapes, dimensions and wavelength using previously verified Mie-based MATLAB code[10] (Table 4). Mie theory was used to model the optical properties of *PNBs*.[80-82] The modeling of the core-shell *NPs* has been performed by analyzing the multilayer structure with the boundary conditions at each metal-dielectric interface considered as a matrix form using *VSWFs*[10]. The vapor bubble is modeled as a concentric geometry consisting of a nanoparticle located in the center surrounding by a spherical layer of air. The entire nanoparticle-bubble system is surrounded by water. Such approach has been recently developed and validated by us.[10,68] In each geometrical region, light is modeled as waves composed of vector spherical wave functions (*VSWFs*). Vector spherical wave functions represent valid solutions to the vector Helmholtz equation and satisfy the divergence-free criterion as in the Maxwell's equations.

The *VSWFs*, denoted as $\overrightarrow{M}$ and $\overrightarrow{N}$, are related to the wave number in the material ^{k}, the radial distance from the origin ^{r}, spherical Hankel functions of the first and second kind, and normalized spherical scalar harmonics (for the angular-dependent components). Vector spherical wave functions of the first kind, $\overrightarrow{M}^{(1)}$ and $\overrightarrow{N}^{(1)}$, are used to represent outgoing waves; *VSWFs* of the second kind, $\overrightarrow{M}^{(2)}_{nm}$ and $\overrightarrow{N}^{(2)}_{nm}$, are used to represent incoming waves; *VSWFs* of the regular kind, $\overrightarrow{M}^{(3)}_{nm}$ and $\overrightarrow{N}^{(3)}_{nm}$, represent waves that are finite at the origin and are defined by:

$$\overrightarrow{M}^{(3)}(kr) = \frac{1}{2}\left[\overrightarrow{M}^{(1)}(kr) + \overrightarrow{M}^{(2)}(kr)\right]$$

$$\overrightarrow{N}^{(3)}(kr) = \frac{1}{2}\left[\overrightarrow{N}^{(1)}(kr) + \overrightarrow{N}^{(2)}(kr)\right].$$

In the outmost region, the incident wave is expanded by $\overrightarrow{M}_{nm}^{(3)}$ and $\overrightarrow{N}_{nm}^{(3)}$ using the multipole expansion coefficients for plane waves. The scattered wave is expanded by $\overrightarrow{M}_{nm}^{(1)}$ and $\overrightarrow{N}_{nm}^{(1)}$ multiplied by Mie scattering coefficients a_n and b_n. In the intermediate layers, waves are expressed by both *VSWFs* of the first and second kind. In the innermost region (either gold nanoparticle or the dielectric core of the nanoshell), waves are represented by regular *VSWFs*. The tangential components of the electric and magnetic waves are equalized across each interface between two adjacent layers owing to the boundary condition. The equations were then solved for the Mie scattering coefficients.

Using Mie coefficients a_n and b_n, the scattering cross section of the nanoparticle-bubble system was calculated as:

$$C_{sca} = \frac{2\pi}{k_o^2} \sum_{n=1}^{\infty} (2n+1) \left(|a_n|^2 + |b_n|^2 \right),$$

where k_o is the wave number of the incident water in water. The upper limit of the index n is truncated at $k_o r_o + 3(k_o r_o)1/3$, with r_o being the radius of *PTB*. The absorption cross section C_{abs} was calculated by subtracting the scattering cross section C_{sca} from the extinction cross section C_{ext}, which can be obtained from Mie coefficients by using:

$$C_{ext} = \frac{2\pi}{k_o^2} \sum_{n=1}^{\infty} (2n+1) \, Re \, (a_n + b_n).$$

For 60 nm hollow gold nanoshell, a refractive index of 1.33 is used for the core. The index of silica, water, and air bubble is 1.43, 1.33 and 1.00, in order. The dielectric function of gold is adapted from Johnson and Christy[83]. It should be noted that the intrinsic effect from surface scattering on nanoparticles is not considered as this model mainly concerns the scattering amplification of the bubble rather than its spectral properties. It is also worth noting that all geometries are assumed to be concentric and rigidly spherical. The assumption of a planar incident wave is valid when the bubble is relatively small compared to the focus spot size of the focusing lens for the probe beam (focal length 200 mm).

Acknowledgments

REFERENCES

1. Liao H, Nehl C, Hafner J. Biomedical Applications of Plasmon Resonant Metal Nanoparticles. Nanomedicine 2006;1:201–208. [PubMed: 17716109]

2. Pitsillides M, Joe E, Wei X, Anderson R, Lin C. Selective Cell Targeting with Light-Absorbing Microparticles and Nanoparticles. Biophys. J 2003;84:4023–4032. [PubMed: 12770906]

3. Loo C, Lowery A, Halas N, West J, Drezek R. Immunotargeted Nanoshells for Integrated Cancer Imaging and Therapy. Nano Lett 2005;5:709–711. [PubMed: 15826113]

4. Tong L, Zhao Y, Huff T, Hansen M, Wei A, Cheng J. Gold Nanorods Mediate Tumor Cell Death by Compromising Membrane Integrity. Adv. Mater 2007;19:3136–3141. [PubMed: 19020672]

5. El-Sayed I, Huang X, El-Sayed M. Selective Laser Photo-Thermal Therapy of Epithelial Carcinoma Using Anti-EGFR Antibody Conjugated Gold Nanoparticles. Cancer Lett 2006;239:129–135. [PubMed: 16198049]

6. Govorov O, Richardson H. generating heat with Metal Nanoparticles. Nano Today 2007;1:30–38.

7. Sokolov K, Follen M, Aaron J, Pavlova I, Malpica A, Lotan R, Richards-Kortum R. Real-Time Vital Optical Imaging of Precancer Using Anti-Epidermal Growth Factor Receptor Antibodies Conjugated to Gold Nanoparticles. Cancer Res 2003;63:1999–2004. [PubMed: 12727808]

8. Yguerabide J, Yguerabide E. Light-Scattering Submicroscopic Particles as Highly Fluorescent Analogs and Their Use as Tracer Labels in Clinical and Biological Applications. II. Experimental characterization. Anal. Biochem 1998;262:157–176. [PubMed: 9750129]

9. Javier D, Nitin N, Roblyer D, Richards-Kortum R. Metal-Based Nanorods as Molecule-Specific Contrast Agents for Reflectance Imaging in 3D Tissues. J. Nanophotonics 2008;2:023506.

10. Hu Y, Fleming R, Drezek R. Optical Properties of Gold-Silica-Gold Multilayer Nanoshells. Opt. Express 2008;16:19579–19591. [PubMed: 19030045]

11. Jingyi, Chen; Fusayo, Saeki; Wiley, B.; Hu, Cang; Cobb, M.; Zhi-Yuan, Li; Au, L.; Hui, Zhang; Kimmey, M.; Xingde, Li, et al. Gold Nanocages: Bioconjugation and Their Potential Use as Optical Imaging Contrast Agents. Nano Lett 2005;5:473–477. [PubMed: 15755097]

12. El-Sayed IH, Huang X, El-Sayed MA. Surface Plasmon Resonance Scattering and Absorption of Anti-EGFR Antibody Conjugated Gold Nanoparticles in Cancer Diagnostics: Applications in Oral Cancer. Nano Lett 2005;5:829–834. [PubMed: 15884879]

13. Hu M, Hartland G. Investigation of the Properties of Gold Nanoparticles in Aqueous Solution at Extremely High Lattice Temperatures. Chem. Phys. Lett 2004;391:220–225.

14. Plech A, Cerna R, Kotaidis V, Hudert F, Bartels A, Dekorsy T. A Surface Phase Transition of Supported Gold Nanoparticles. Nano Lett 2007;13:17352505.

15. Inasawa S, Sugiyama M, Noda S, Yamaguchi Y. Spectroscopic study of Laser-Induced Phase Transition of Gold Nanoparticles on Nanosecond Time Scales and Longer. J. Phys. Chem. B 2006;110:3114–3119. [PubMed: 16494317]

16. Petrova H, Min H, Hartland GZ. Photothermal Properties of Gold Nanoparticles. Phys. Chem. B 2007;221:361–376.

17. Jain P, Lee K-S, El-Sayed IH, El-Sayed MA. Calculated Absorption and Scattering Properties of Gold Nanoparticles of Different Size, Shape, and Composition: Applications in Biological Imaging and Biomedicine. J. Phys. Chem. B 2006;110:7238–7248. [PubMed: 16599493]

18. Prodan E, Lee A, Nordlander P. The Effect of a Dielectric Core and Medium on the Polarizability of Metallic Nanoshells. Chem. Phys. Lett 2002;360:325–332.

19. Tam F, Moran C, Halas N. Geometrical Parameters Controlling Sensitivity of Nanoshell Plasmon Resonances to Changes in Dielectric Environment. J. Phys. Chem. B 2004;108:17290–17294.

20. Tam F, Halas N. Plasmon Response of Nanoshell Dopants in Organic Films: a Simulation Study. Prog. Org. Coat 2003;47:275–278.

21. Keblinski P, Cahill D, Bodapati A, Sullivan C, Taton TA. Limits of Localized Heating by Electromagnetically Excited Nanoparticles. J. Appl. Phys 2006;100:054305.

22. Volkov A, Sevilla C, Zhigilei L. Numerical Modeling of Short Pulse Laser Interaction with Au Nanoparticle Surrounded by Water. Appl. Surf. Sci 2007;253:6394–6399.

23. Hartland G. Measurement of the Material Properties of Metal Nanoparticles by Time-Resolved Spectroscopy. Phys. Chem. Chem. Phys 2004;6:5263–5274.

24. Perez-Juste J, Pastoriza-Santos I, Liz-Marzan LM, Mulvaney P. Gold Nanorods: Synthesis, Characterization and Applications. Coord. Chem. Rev 2005;249:1870–1901.

25. Yguerabide O, Yguerabide E. Light-Scattering Submicroscopic Particles as Highly Fluorescent Analogs and Their Use as Tracer Labels in Clinical and Biological Applications. Anal. Biochem 1998;262:137–156. [PubMed: 9750128]

26. Vogel A, Linz N, Freidank S, Paltauf G. Femtosecond-Laser-Induced Nanocavitation in Water: Implications for Optical Breakdown Threshold and Cell Surgery. Phys. Rev. Lett 2008;100:038102. [PubMed: 18233040]

27. Vogel A, Noack J, Hüttmann G, Paltauf G. Mechanisms of Femtosecond Laser Nanosurgery of Cells and Tissues. Appl. Phys. B 2005;81:1015–1047.

28. Neumann J, Brinkmann R. Nucleation Dynamics Around Single Microabsorbers in Water Heated by Nanosecond Laser Irradiation. J. Appl. Phys 2007;101:114701.

29. Neumann J, Brinkmann R. Boiling Nucleation on Melanosomes and Microbeads Transiently Heated by Nanosecond and Microsecond Laser Pulses. J. Biomed. Opt 2005;10:024001. [PubMed: 15910075]

30. Marston, PL. Light scattering by bubbles in liquids and its applications to physical acoustics. In: Crim, LA., et al., editors. Sonochemistry and Sonoluminescence. Kluwer Academic Publishers; 1999. p. 73-86.

31. Yavas O, Leiderer P, Park H, Grigoropoulos C, Poon C, Leung W, Do N, Tam A. Optical Reflectance and Scattering Studies of Nucleation and Growth of Bubbles at a Liquid-Solid Interface Induced by Pulsed Laser Heating. Phys. Rev. Lett 1993;70:1830–1833. [PubMed: 10053397]

32. Lauterborn W, Bolle H. Experimental Investigations of Cavitation-Bubble Collapse in The Neighbourhood of a Solid Boundary. J. Fluid Mech 1975;72:391–399.

33. Shima A. Studies on Bubble Dynamics. Shock Waves 1997;7:33–42.

34. Carey, VP. Liquid–Vapor Phase Phenomena. Hemisphere Pub. Corp.; Washington, D.C.: 1992.

35. Asshauer T, Rink K, Delacrétaz G. Acoustic Transient Generation by Holmium-Laser-Induced Cavitation Bubbles. J. Appl. Phys 1994;76:5007–5013.

36. Lin CP, Kelly MW. Cavitation and Acoustic Emission Around Laser-Heated Microparticles. Appl. Phys. Lett 1998;72:2800–2802.

37. Lin CP, Kelly MW, Sibayan SAB, Latina MA, Anderson RR. Selective Cell Killing by Microparticle Absorption of Pulsed Laser Radiation. IEEE J. Quantum Electron 1999;5:963–968.

38. van Leeuwen TG, Jansen ED, Welch AJ, Borst C. Excimer Laser Induced Bubbles: Dimensions, Theory and Implications for Laser Angioplasty. Lasers Surg. Med 1996;4:381–390. [PubMed: 8732577]

39. Hutson S, Ma X. Plasma and Cavitation Dynamics During Pulsed Laser Microsurgery *in vivo*. Phys. Rev 2007;99:158104.

40. Heisterkamp A, Maxwell IZ, Mazur E, Underwood JM, Nickerson JA, Kumar S, Ingber DE. Pulse Energy Dependence of Subcellular Dissection by Femtosecond Laser Pulses. Opt. Express 2005;13:3690–3696. [PubMed: 16035172]

41. Farny H, Wu T, Holt RG, Murray TW, Roy RA. Nucleating Cavitation from Laser-Illuminated Nano-Particles. Acoust. Res. Lett. Online 2005;6:138–143.

42. Kotaidis V, Plech A. Cavitation Dynamics on the Nanoscale. Appl. Phys. Lett 2005;87:213102.

43. Kotaidis V, Dahmen C, von Plessen G, Springer F, Plech A. Excitation of Nanoscale Vapor Bubbles at the Surface of Gold Nanoparticles in Water. J. Chem. Phys 2006;124:184702. [PubMed: 16709126]

44. François L, Mostafavi M, Belloni J, Delaire J. Optical Limitation Induced by Gold Clusters: Mechanism and Efficiency. Phys. Chem 2001;3:4965–4971.

45. Hleb E, Lapotko D. Photothermal Properties of Gold Nanoparticles under Exposure to High Optical Energies. Nanotechnology 2008;19:355702.

46. Lapotko D. Optical Excitation and Detection of Vapor Bubbles Around Plasmonic Nanoparticles. Opt. Express 2009;17:2538–2556. [PubMed: 19219157]

47. Lapotko D, Lukianova K. Laser-Induced Micro-Bubbles in Cells. Int. J. Heat Mass Transfer 2005;48:227–234.

48. Lapotko D. Pulsed Photothermal Heating of the Media During Bubble Generation Around Gold Nanoparticles. Int. J. Heat Mass Transfer 2009;52:1540–1543.

49. van Leeuwen TG, Jansen ED, Motamedi M, Welch AJ, Borst C. Excimer Laser Ablation of Soft Tissue: a Study of the Content of Rapidly Expanding and Collapsing Bubbles. IEEE J. Quantum Electron 1994;30:1339–1345.

50. Rayleigh L. On the Pressure Developed in a Liquid During the Collapse of a Spherical Cavity. Philos. Mag 1917;34:94–98.

51. Brennen, CE. Cavitation and bubble dynamics. Oxford University Press, Oxford Engineering Science; NY: 1995. p. 44

52. Ohl C-D, Kurz T, Geisler R, Lindau O, Lauterborn W. Bubble Dynamics, Shock Waves and Sonoluminescence. Philos. Trans. R. Soc. London, Ser. A 1999;357:269–294.

53. Dou Y, Zhigilei LV, Winograd N, Garrison BJ. Explosive Boiling of Water Films Adjacent to Heated Surfaces: A Microscopic Description. J. Phys. Chem. A 2001;105:2748–22755.

54. Perigaud G, Saurel R. A compressible flow model with capillary effects. J. Comp. Phys 2005;209:139–2178.

55. Wagner W, Pruß A. The IAPWS formulation 1995 for the thermodynamic properties of ordinary water substance for general and scientific use. J. Phys. Chem. Ref. Data 2002;31:387–535.

56. Merabia S, Keblinski P, Joly L, Lewis LJ, Barrat J-L. Critical Heat Flux Around Strongly Heated Nanoparticles. Phys. Rev. E 2009;79:021404.

57. Merabia S, Shenogin S, Joly L, Keblinski P, Barrat J-L. Heat Transfer from Nanoparticles: A Corresponding State Analysis. Proc. Natl. Acad. Sci. U. S. A 2009;106:15113–15118. [PubMed: 19571000]

58. Garrison BJ, Itina TE, Zhigilei LV. The Limit of Overheating and the Threshold Behavior in Laser Ablation. Phys. Rev. E 2003;68:041501.

59. Xu, X. Phase Change Mechanisms in Pulsed Laser-Matter Interaction. Ultrafast Lasers for Materials Science; Materials Research Society Symposium Proceedings; 2005. p. 3-12.

60. Hleb EY, Hafner JH, Myers JN, Hanna EY, Rostro BC, Zhdanok SA, Lapotko DO. LANTCET: elimination of solid tumor cells with photothermal bubbles generated around clusters of gold nanoparticles. Nanomedicine 2008;3:647–667. [PubMed: 18817468]

61. Asshauer T, Delacretaz G, Jansen ED, Welch AJ, Frenz M. Pulsed holmium laser ablation of tissue phantoms: correlation between bubble formation and acoustic transients. Appl. Phys. B 1997;65:647–657.

62. de Gennes, PG.; Françoise, B-W.; Quéré, D. Capillary and Wetting Phenomena — Drops, Bubbles, Pearls, Waves. Springer; 2002.

63. Dean, JA., editor. Lange's Handbook of Chemistry. 15th ed. McGraw-Hill; New York: 1998. p. 1661-1665.

64. Adamson, AW.; Gast, AP. Physical chemistry of surfaces. 6th ed. Wiley Interscience; 1997.

65. Anderson R, Parrish J. Selective Photothermolysis: Precise Microsurgery by Selective Absorption of Pulsed Radiation. Science 1983;220:524–527. [PubMed: 6836297]

66. Lee S, Anderson T, Zhang H, Flotte TJ, Doukas AG. Alteration of Cell Membrane by Stress Waves *in vitro*. Ultrasound Med. Biol 1996;22:1285–1293. [PubMed: 9123654]

67. Lapotko D, Hleb E. Influence of Transient Environmental Photothermal Effects on Optical Scattering by Gold Nanoparticles. Nano Lett 2009;9:2160–2166. [PubMed: 19374436]

68. Hleb EY, Hu Ying, Drezek RA, Hafner JH, Lapotko DO. Photothermal Bubbles as Optical Scattering Probes for Imaging Living Cells. Nanomedicine 2008;3:797–812. [PubMed: 19025454]

69. Huttmann G, Birngruber R. On the Possibility of High-Precision Photothermal Microeffects and the Measurement of Fast Thermal Denaturation of Proteins. IEEE J. Sel. Top. Quantum Electron 1999;5:954–962.

70. Kelly, MW. Ph.D. dissertation. Tufts Univ.; Medford, MA: 1997. Intracellular cavitation as a mechanism of short-pulse laser injury of the retinal pigment epithelium.

71. Wu T-H, Kalim S, Callahan C, Teitell MA, Chiou P-Y. Image Patterned Molecular Delivery Into Live Cells Using Gold Particle Coated Substrates. Opt. Express 2010;18:938–946. [PubMed: 20173916]

72. Hu M, Petrova H, Hartland GV. Investigation of the Properties of Gold Nanoparticles in Aqueous Solution at Extremely High Lattice Temperatures. Chem. Phys. Lett 2004;391:220–225.

73. Neumann J, Brinkmann R. Microbubble Dynamics Around Laser Heated Microparticles. Proc. SPIE-Int. Soc. Opt. Eng 2003;5142:82–87.

74. Brinkmann R, Neumann J. Self-limited growth of laser-induced vapor bubbles around single microabsorbers. Appl. Phys. Lett 2008;93:033901.

75. Kozuka T, Hatanaka S-I, Yasui K, Tuziuti T, Mitome H. Simultaneous Observation of Motion and Size of a Sonoluminescing Bubble. Jpn. J. Appl. Phys 2002;41:3248–3249.

76. Stöber W, Fink A, Bohn E. Controlled Growth of Monodisperse Silica Spheres in the Micron Size Range. J. Colloid Interface Sci 1968;26:62–69.

77. Turkevitch J, Stevenson PC, Hillier J. Nucleation and Growth Process in the Synthesis of Colloidal Gold. Discuss. Faraday Soc 1951;11:55–75.

78. Wiley B, Sun Y, Mayers B, Xia Y. Shape-Controlled Synthesis of Metal Nanostructures: The Case of Silver. Chem. Eur. J 2005;11:454–463.

79. Toro, EF. Riemann Solvers and Numerical Methods for Fluid Dynamics. Springer; Berlin: 1999.

80. Revised Release on the IAPS Formulation 1985 for the Thermal Conductivity of Ordinary Water Substance. International Association for the Properties of Water and Stream; 1998. http://www.iapws.org/

81. van de Hulst, HC. Light Scattering by Small Particles. Wiley; New York: 1957.

82. Bohren, CF.; Huffman, DR. Absorption and Scattering of Light by Small Particles. Wiley Interscience; New York: 1983.

83. Johnson PB, Christy RW. Optical Constants of the Nobel Metals. Phys. Rev. B 1972;6:4370–4379.
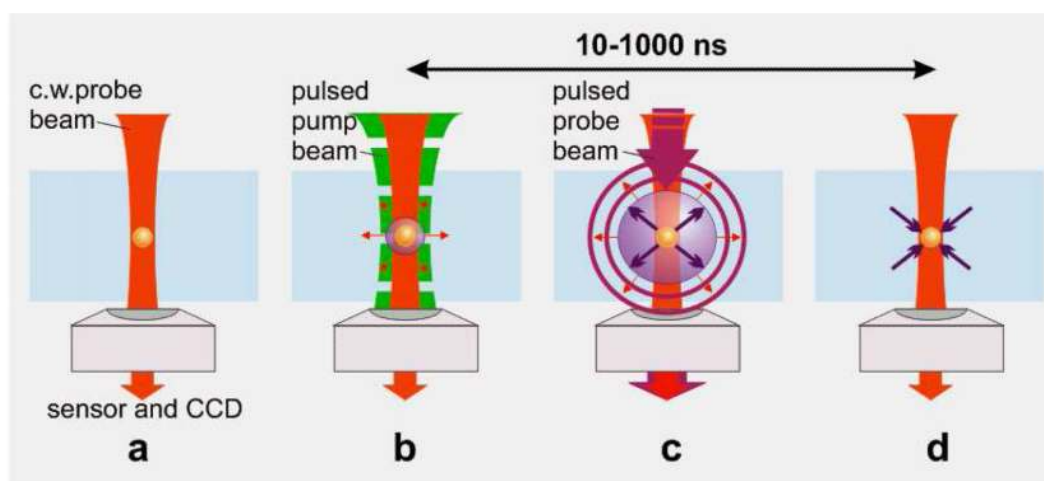
Figure 1.
Optical generation and detection of plasmonic nanobubbles: (a) gold *NP* in water is imaged with a low power probe laser beam (633 nm); (b) *NP* is exposed to a short pump laser pulse at specific fluence above (0.5 ns, 532 nm), that at the first stage produces the vapor layer around heated *NP*; (c) at the second stage when the pressure inside the vapor layer exceeds the outer pressure the vapor begins to expand into a bubble, which is detected with the two probe lasers (red and purple): scattering by the bubble forms the image and the time response; (d) a bubble collapses at the end of its lifespan (10-1000 ns).
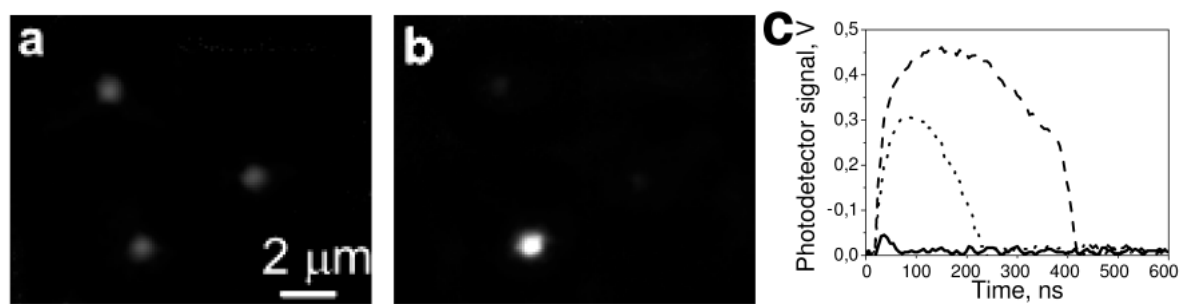
Figure 2.
Optical pulsed side-scattering images of (a) three 250 nm gold spheres in water, (b) transient vapor bubble generated around one *NP* positioned to the center of pump laser beam, (c) optical scattering time responses at the level of pump pulse fluence (0.13 J/cm^2) for 250 nm gold sphere (solid), 250/15 nm silica-gold shell (dot) and for the cluster of gold shells (dash).
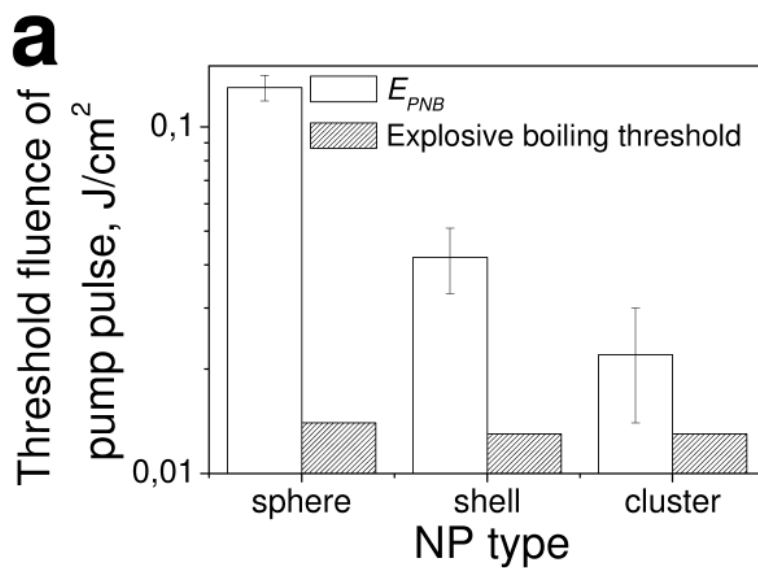
Figure 3.
Observed thresholds for the bubble generation (E_{PNB}) and estimated thresholds for explosive boiling around single gold *NPs* (250 nm solid sphere and silica-gold shell) and around shell clusters. Data are shown for a single excitation pump laser pulse (0.5 ns, 532 nm).
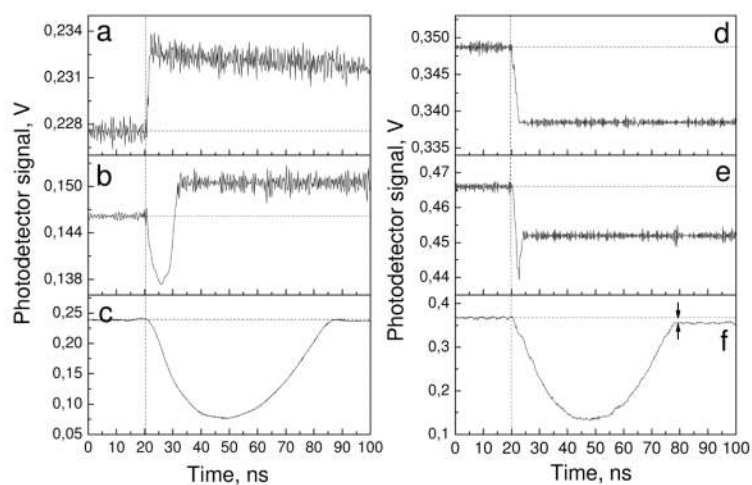
Figure 4.
Time responses for single 80-nm gold nanoparticles (a-c) and molecular solution of Trypan Blue (d-f) obtained with a single pump laser pulse (vertical dashed line) near the *PNB* threshold fluences. Two arrows in f show the deviation of the after bubble signal from the baseline due to residual heating of the surrounding water.
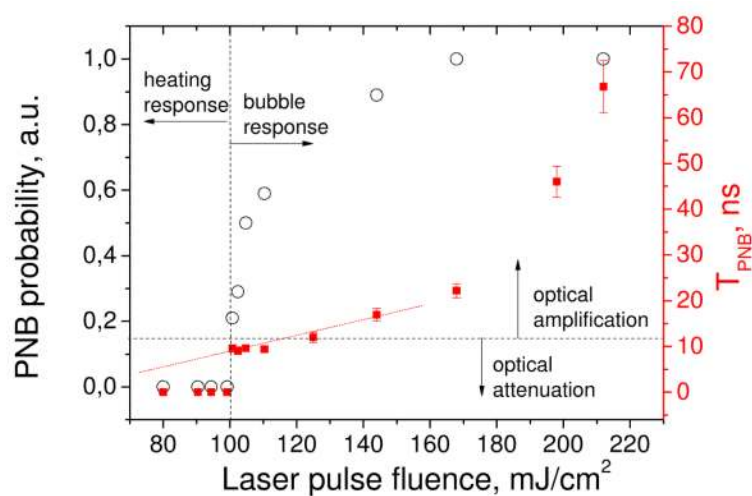
Figure 5.
Dependence of the *PNB* lifetime (T_{PNB}, red) and the generation probability (black) around single 90 nm gold spheres upon the fluence of a single pump laser pulse (0.5 ns, 532 nm); vertical line separates the types of corresponding time responses (Figure 4) and the horizontal line separates the optical scattering effect.
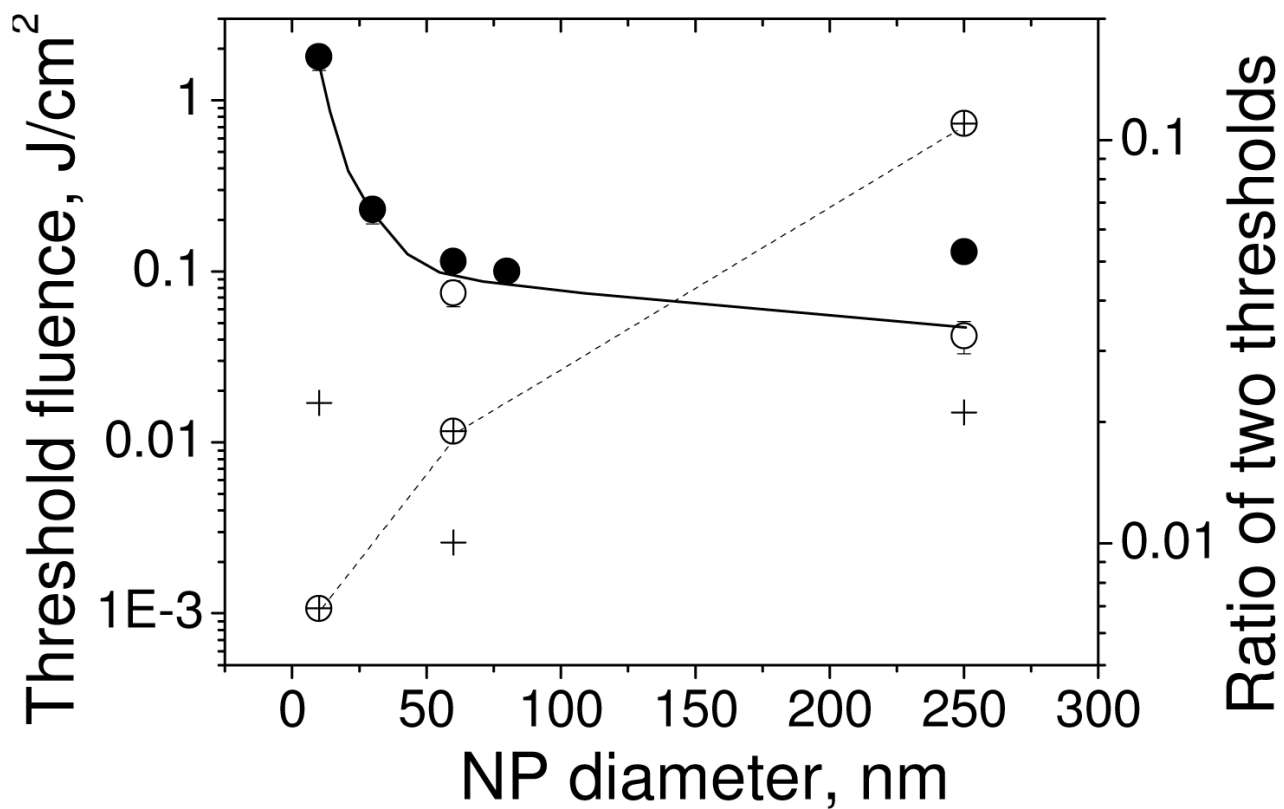
Figure 6.
Threshold fluences of pump laser pulse (0.5 ns, 532 nm) for the explosive boiling (+ −
calculated for spheres) and bubble generation (measured for ● – spheres and ○ – shells,) as
functions of the diameter of gold NPs, solid line shows the bubble generation threshold
trend, dashed line shows the trend for the ratio of explosive boiling threshold to bubble
generation threshold (right Y axis).
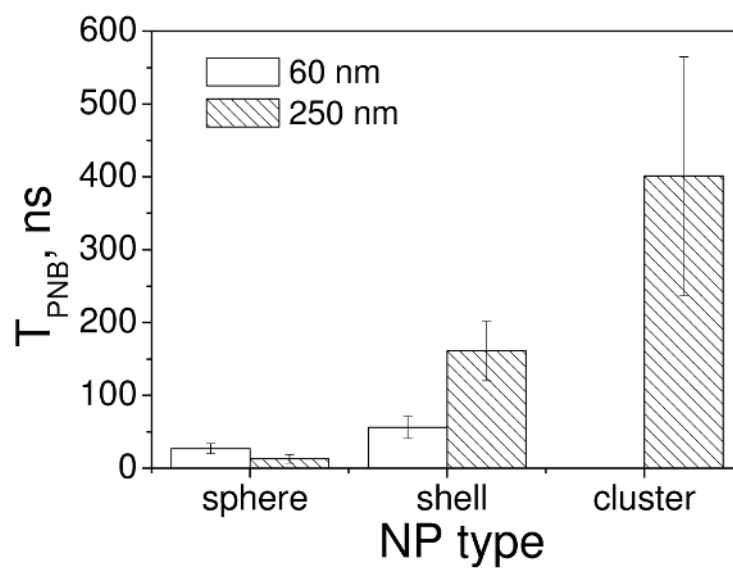
Figure 7.
Lifetimes of the *PNBs* (*T_PNB*) generated around individual *NPs* (gold spheres and shells of 60 nm and 250 nm diameter) and around NP (shell) clusters at the fluence of the pump laser pulse 0.13 J/cm^2.
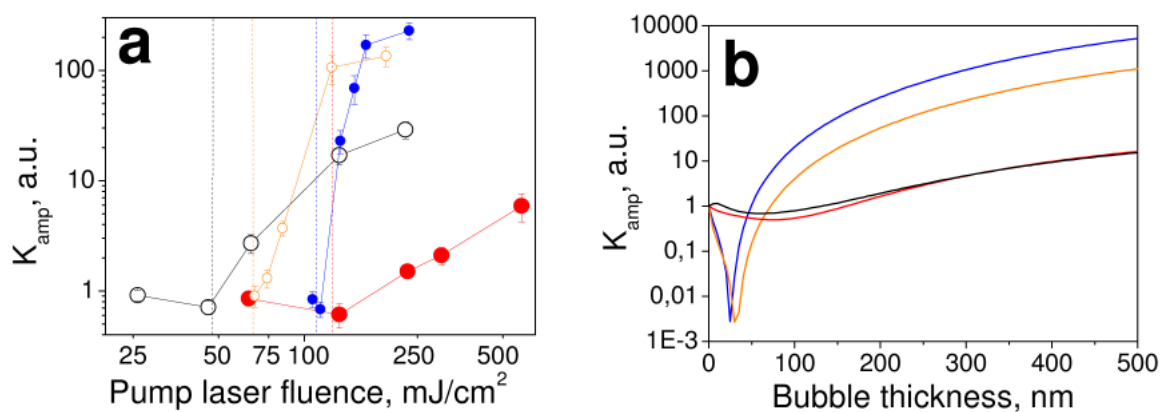
Figure 8.
Experimental (a) and theoretical (b) data on optical scattering by the nanoparticle-bubble system: (a) optical scattering amplification coefficient as function of pump pulse (0.5 ns, 532 nm) fluence: hollow black circle – 250 nm shells, red circle – 250 nm spheres, blue circle – 60 nm spheres, hollow orange circle – 60 nm shells, dashed vertical lines show the corresponding bubble generation thresholds; (b) optical scattering amplification coefficient calculated as the function of the bubble thickness (the difference in radii of the *PNB* and *NP*).
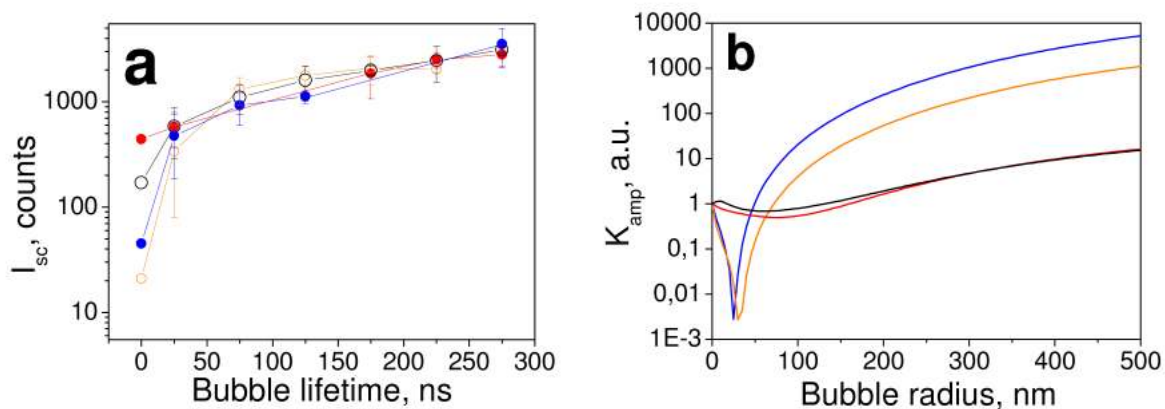
Figure 9.
Experimental (a) and theoretical (b) data on optical scattering by the nanoparticle-bubble system: (a) pixel image amplitude of the bubble measured as function of the bubble lifetime (T_{PNB}): optical scattering amplification coefficient as function of pump pulse (0.5 ns, 532 nm) fluence: hollow black circle – 250 nm shells, red circle – 250 nm spheres, blue circle – 60 nm spheres, hollow orange circle – 60 nm shells; (b) calculated optical scattering cross section of the nanoparticle-bubble system as function of the bubble radius.
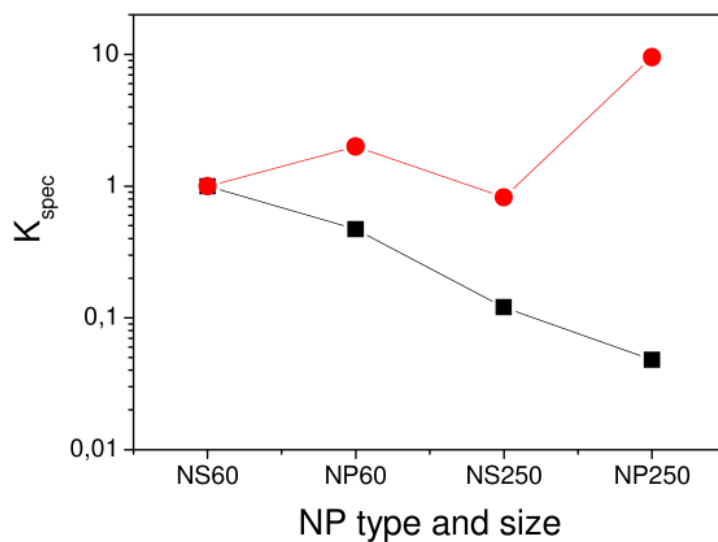
Figure 10.
Optical contrast coefficients for 60 nm shell (black squares)) and the corresponding *PNB* (red circles) generated around it at 0.13 J/cm^2 as compared to other *NPs* (NS60 - 60 nm shells, NP60 – 60 nm spheres, NS250 - 250 nm shells, NP250 - 250 nm spheres) and the *PNBs* generated around them under identical conditions.
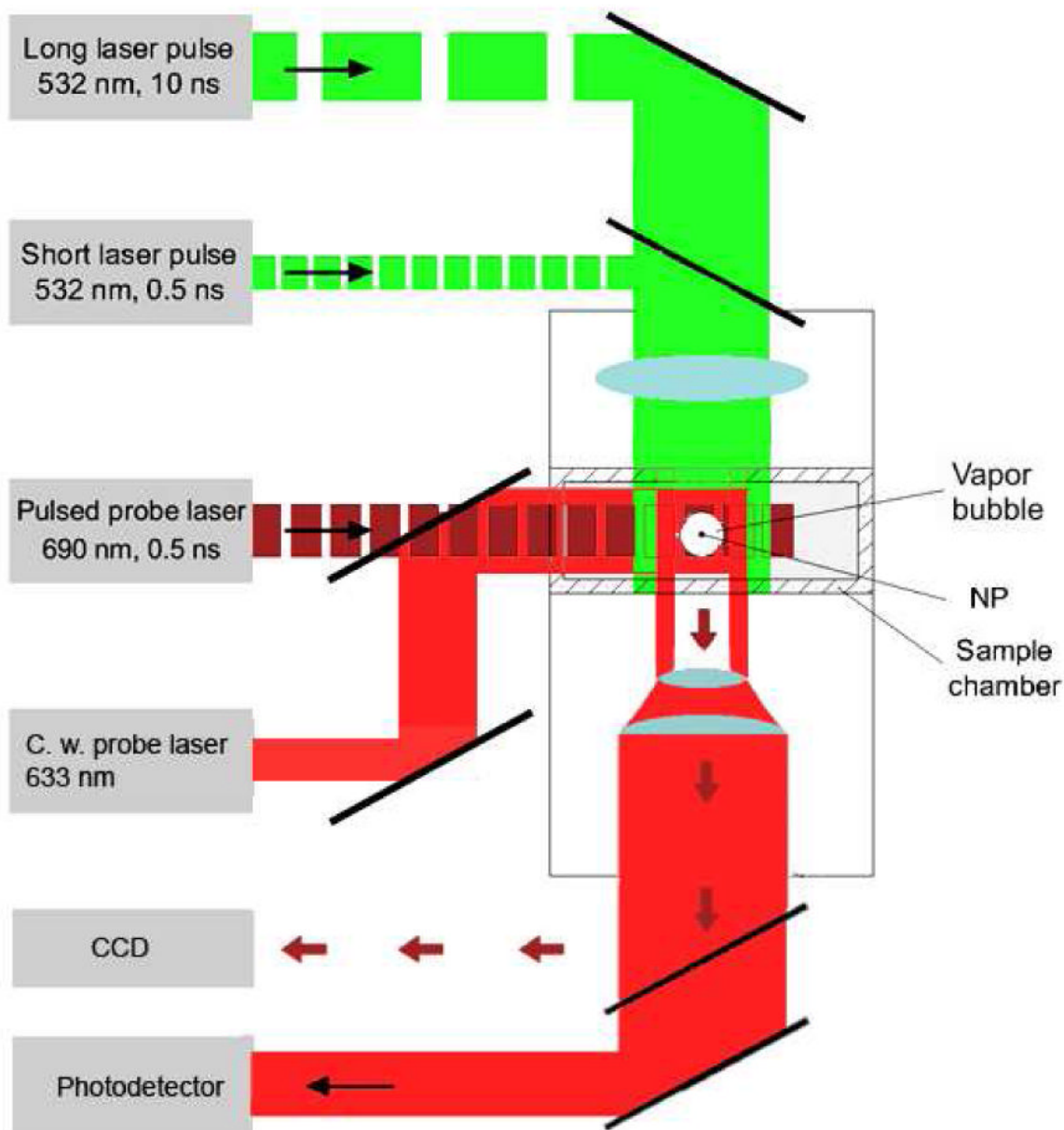
Figure 11.
Experimental setup: single gold *NPs* in water were placed in the sample chamber mounted
on the microscope stage; bubble generation was provided by focused single pulses (532 nm,
05 ns or 10 ns); a pulsed probing laser (690 nm, 05 ns) provided time-resolved optical
scattering imaging of bubble and a continuous probing laser (633 nm, 1 mW) provided the
monitoring of the integral optical scattering of bubble.

Table 1

The influence of the duration of optical excitation (532 nm) on the explosive boiling and bubble generation thresholds (E_{PNB}) and lifetimes (T_{PNB}) for 250 nm gold shells.

Duration of optical excitation	0.5 ns	10 ns	Continuous (100 s)
E_{PNB}, J/cm^2 (measured)	0.042 ±0.009	0.4±0.04	-
Explosive boiling threshold (calculated)	0.013 J/cm^2	0.043 J/cm^2	380 kW/cm^2
Ratio for explosive boiling threshold/ E_{PNB}	0.31	0.1	-
T_{PNB}@0.6 J/cm^2, ns (measured)	690±138	65±12	0

Table 2

Optical scattering properties of gold *NPs* and *NP*-generated bubbles

Nanoparticle type	Gold spheres		Gold shells	
NP diameter, nm	60 nm	250 nm	60 nm	250 nm
I_{sc} (0), counts	45±11	440±58	21±10	170±83
K_{ampl} @ 0.13 J/cm^2	27	0.57	113	17
I_{sc} @ T_{PNB}175 ns, counts	2040±289	1856±216	2087±261	1990±294

Table 3

Comparison of the properties of plasmonic nanoparticles and plasmonic nanobubbles.

Properties	Thermal	Mechanical	Optical	Threshold	Temporal nature
Nanoparticle	Thermal diffusion	Acoustic wave	Constant scattering	–	Steady
Nanobubbl	Thermal impact is confined inside PNB thermal impact	Tunable and localized expansion	Tunable scattering	+	Transient

Table 4

Calculated absorption (C_{abs}) and scattering (C_{sca}) cross-sections of the gold *NP* employed in the experiments.

	250 nm silica-gold core-shell nanoshell	250 nm gold nanosphere	60 nm hollow nanoshell	60 nm gold nanosphere	10 nm gold nanosphere	80 nm gold nanosphere
C_{abs} @ 532 nm, m^2	3.55e-14	6.81e-14	2.81e-15	1.12e-14	4.65e-17	1.84e-14
C_{sca} @ 690 nm, m^2	1.73e-13	1.69e-13	2.36e-15	3.46e-16	5.83e-21	2.32e-15